



# Deep desulfurization of liquid fuels with molecular oxygen through graphene photocatalytic oxidation



Xingye Zeng<sup>a,b</sup>, Xinyan Xiao<sup>a,\*</sup>, Yang Li<sup>a</sup>, Jiayi Chen<sup>a</sup>, Hanlu Wang<sup>b</sup>

<sup>a</sup> School of Chemistry and Chemical Engineering, South China University of Technology, Guangzhou, 510640, PR China

<sup>b</sup> College of Chemical Engineering, Guangdong University of Petrochemical Technology, Maoming, 525000, PR China

## ARTICLE INFO

### Article history:

Received 31 December 2016

Received in revised form 23 February 2017

Accepted 27 February 2017

Available online 1 March 2017

### Keywords:

Graphene oxide

Photocatalytic oxidative desulfurization

Extraction

Dibenzothiophene

Density functional theory

## ABSTRACT

A simple extraction and photocatalytic oxidative desulfurization (EPODS) system for model oil was successfully developed on the basis of as-prepared graphene oxide (GO), air, formic acid (MeA), and acetonitrile (MeCN). Under UV radiation, the main reaction conditions influencing sulfur removal were systematically investigated, including the amount of GO, the volume ratio of MeCN to model oil, the amount of MeA, the initial S-concentration, air/N<sub>2</sub> bubbling, different sulfur compounds, and fuel composition. The reactivities of different sulfur compounds decreased in the order of benzothiophene > dibenzothiophene (DBT) > 4,6-dimethylbenzothiophene, and this was attributed to the influences of the electronic structure of the lowest-lying triplet state of each species and to steric hindrance. The photocatalytic oxidative desulfurization mechanism was investigated using radical scavenger experiments, gas chromatography-mass spectrometry, electron spin-resonance spectroscopy, and density functional theory. DBT was initially extracted into the MeCN phase and then oxidized to the mixed oxidation products including sulfone. This was accomplished by the produced HO<sub>2</sub><sup>•</sup> and HO<sup>•</sup>, which mainly originated from the oxygen-containing functional groups with absorbed O<sub>2</sub>, ambient H<sup>+</sup>, and the additional electrons at the zigzag edge and at the defect sites of GO. This work presents a promising approach to the highly-efficient removal of heterocyclic aromatic sulfur compounds from liquid fuels with an ultra-low dosage of carbon catalyst under mild conditions. Additionally, it provides insights into the fundamental knowledge on the origin of GO activity and the nature of the active oxygen functional groups in the photocatalytic process.

© 2017 Elsevier B.V. All rights reserved.

## 1. Introduction

Liquid fuels are widely used both in the generation of electricity and in various transportation systems (e.g. cars, buses, trucks, and marine vessels) [1]. Sulfur compounds in liquid fuels poison the catalysts in emission control systems in vehicles and convert to sulfur dioxide during combustion resulting in acid rain and serious haze [2]. To reduce air pollution, increasingly stringent regulations have been imposed worldwide to limit the sulfur content of fuels to a very low level [3]. For instance, according to the standard JIS K 2202, Japan has restricted the sulfur content of motor gasoline to be less than 10 ppm since 2007. In the U.S., the sulfur content limit of highway diesel was reduced from 15 ppm to less than 10 ppm at the beginning of 2017 [4,5]. At the same time, China has executed

the V generation vehicle gasoline and diesel standards program, which limits the sulfur content of regular gasoline and diesel fuels from 50 ppm to less than 10 ppm.

To meet the quality demands of liquid fuels with ultra-low sulfur content (<10 ppm of S content), hydrodesulfurization (HDS) has been a classic technology used by refineries. HDS takes a series of measures for deep removal of sulfur compounds and has included expensive hydrotreating catalysts and harsh process parameters such as temperature >370 °C and pressure >40 atm [6]. As a result, these measures not only increase extra operating and investment costs, but also cause quality loss of liquid fuel under high temperature. However, HDS is still less efficient at removing heterocyclic aromatic sulfur compounds (HASCs) such as benzothiophene (BT), dibenzothiophene (DBT), and 4,6-dimethylbenzothiophene (4,6-DMDBT) because of their lower hydrogenation activity and steric hindrance [7]. Consequently, more attention has been paid to non-HDS methods and their combined forms, such as extractive desulfurization [8], biodesulfurization [9], oxidative desulfurization (ODS) [10–12], and adsorptive desulfurization (ADS) [13–15].

\* Corresponding author.

E-mail addresses: [cexy>xiao@scut.edu.cn](mailto:cexy>xiao@scut.edu.cn) (X. Xiao), [wanglu@mail2.sysu.edu.cn](mailto:wanglu@mail2.sysu.edu.cn) (H. Wang).

Among the aforementioned non-HDS methods, the ODS method has gained enormous interest from the scientific community worldwide because of its lower investment and operating costs, mild reaction conditions, and simpler process [16]. Generally, an effective ODS system consists of an oxidant, a catalyst, and either an extractant or an adsorbent. The sulfur compounds are oxidized to highly polarized sulfones, which can be easily removed by extraction or absorption [17]. Up to now, the ODS method has been developed in a variety of forms, including extraction coupled with thermocatalytic ODS, microbial ODS, photocatalytic ODS, and photochemical ODS [18].

Several oxidants, such as molecular oxygen ( $O_2$ ) [19], hydrogen peroxide [20], ozone [21,22], and *tert*-butyl hydroperoxide [23,24] have been used in previous ODS studies. Although  $O_2$  is undoubtedly the most cost-effective and most highly abundant oxidant, it is inactive because its ground state is a low-energy triplet ( $^3O_2$ ). To activate  $O_2$  for the desulfurization of liquid fuels, earlier thermocatalytic ODS studies focused on using metal-containing catalysts, such as V-Mo [19], Mn-Co [25,26], Fe [27], Pd [28], Co-Mo [29], and Mo [30,31]. However, these reactions have to be carried out with either pure  $O_2$  and/or at high temperatures, or with a long reaction time. In response to these problems, photocatalytic ODS has been considered to be an effective alternative method. Some metal-based photocatalysts, such as CuW/TiO<sub>2</sub>-graphene oxide (GO) [18], Pt–RuO<sub>2</sub>/BiVO<sub>4</sub> [32], Pt–RuO<sub>2</sub>/TiO<sub>2</sub> [33], and Cu–Fe/TiO<sub>2</sub> [34], have been used in photocatalytic ODS systems. However, their high-cost and complicated production processes seriously limit further practical applications. As a result, metal-free photocatalytic methods have attracted extra attention [35].

Recently, the emergence of carbon materials (e.g., graphene, GO, and carbon nanotubes) provides an excellent alternative to metal-containing catalysts in various catalysis fields [36,37]. As promising metal-free catalysts, graphene (GR) and GO have attracted more attention for fuel desulfurization because of their high specific surface areas and special layer structure. In particularly, GO contains both aromatic ( $sp^2$ ) and aliphatic ( $sp^3$ ) domains, which easily form  $\pi$ -complexes with aromatic sulfurs and supply active sites because of the oxygen-containing functional groups. Up to now, GR and GO have been widely used for ADS and ODS [38–41]. For instance, Gonçalves et al. found that three-dimensional GO foam was a promising catalyst for the oxidation of thioanisole with  $H_2O_2$  as an oxidant at room temperature [41]. However, most of these studies focus on ADS, which suffers from a limited absorption capacity to process a large number of S-containing fuel oils. A few studies on ODS use explosive oxidants such as  $H_2O_2$ , which challenge the strict fire safety regulations at refineries. To the best of our knowledge, until now only limited studies have been done to activate  $O_2$  with GO to remove sulfur compounds from fuels. Therefore, developing a deep ODS system using the unique characteristics of GO with environmentally friendly and inexpensive  $O_2$  is a promising technology in terms of sustainability and the green chemical industry.

Although GO has been widely used in various catalysis fields [36], its structure, composition, and role in reaction have not been fully understood. According to the Account reported by Loh et al. [42], the well-accepted structural models of GO depict hydroxyl and epoxide groups as the primary functional groups present on the basal plane. A number of potential active sites allow GO to function as a solid acid or as a green oxidant. In some catalytic oxidation reactions, it is still difficult to determine exactly whether GO is a catalyst or an oxidant [43]. Additionally, the enhanced photocatalytic effect is also ambiguous in GO and dye systems, and this is attributed to the interaction between GO and the dye, or the inherent high surface area and excellent electron transfer capability of GO [44]. These issues are still difficult to eliminate, largely because of the lack of knowledge on the origin of GO activity and the nature of the active oxygen functional groups participating in the reaction

[45]. In general, monitoring the reaction intermediates formed on the surface of GO represents a possible platform for understanding the reaction pathway and mechanism. However, it is difficult to observe *in situ* these adsorbed species because of their extremely short lifetimes. Herein, computational quantum chemistry using on density functional theory (DFT) was employed to predict the possible intermediates formed during the desulfurization reaction process and to evaluate their stabilities.

In this work, a simple extraction and photocatalytic oxidative desulfurization (EPODS) system was investigated. The system was composed of GO, air, formic acid (MeA), and acetonitrile (MeCN) for the deep removal of sulfur compounds from model oil. Sulfur compounds in model oil were extracted in the MeCN phase and oxidized to high-polarity products by the reactive oxygen species (ROS) under UV radiation, achieving deep desulfurization. The main parameters influencing desulfurization performance were examined in detailed, such as the amount of GO, the amount of MeA, the volume ratio of MeCN to model oil ( $r_{M/O}$ ), the initial S-concentration, air/N<sub>2</sub> bubbling, different sulfur compounds, and fuel composition. Moreover, radical scavenger experiments, electron spin-resonance spectroscopy (ESR), gas chromatography-mass spectrometry (GC-MS), and DFT calculations were employed to investigate the mechanism of the EPODS system to establish a base of detailed knowledge for the desulfurization of fuels through GO photocatalytic oxidation.

## 2. Experimental section

### 2.1. Materials

BT (98%), DBT (98%), and 4,6-DMDBT (98%) were purchased from Wuhan Greatwall chemical Sci-Tech development Co. Ltd (China). Other chemical reagents were purchased from Tianjin Kermel Chemical Reagent Co., Ltd (China). All chemicals were analytical reagent grade and used without further purification.

### 2.2. Preparation and characterization

GO was prepared from commercial graphite powder (Tianjin Kermel Fine Chemical Corporation, China) using the modified Hummers method. Graphite powder (2.0 g) and NaNO<sub>3</sub> (1.0 g) were dispersed in 60 mL of 98% H<sub>2</sub>SO<sub>4</sub> in a flask held in an ice bath. After stirring for 1 h in the ice bath, KMnO<sub>4</sub> (6.5 g) was slowly added to the above mixture in a 7 °C water bath. After stirring for 24 h in the water bath, the flask was transferred to a 38 °C water bath for 0.5 h, and 10% H<sub>2</sub>SO<sub>4</sub> (80 mL) was slowly added to the suspension. The temperature was increased to 95 °C, and deionized water (65 mL) was slowly added to the suspension, which was removed from the water bath after 0.5 h and 30% H<sub>2</sub>O<sub>2</sub> (35 mL) and 10% HCl (40 mL) were added. The suspension was diluted with 420 mL of deionized water.

Transmission electron microscope (TEM) imaging was conducted on a FEI Tecnai G2 F20 TEM operating at 200 kV. X-ray photoelectron spectroscopy (XPS) measurements were performed using a multifunctional imaging electron spectrometer (Thermo ESCALAB 250XI) with Al Ka radiation. Attenuated total reflectance Fourier-transform infrared (ATR FT-IR) measurements were carried out using a Nicolet iN10. Raman spectra were recorded on a Laser confocal micro-Raman spectrometer (Horiba Jobin Yvon LabRAM HR800) with a 514.3 nm Ar laser. The X-band ESR spectra were recorded at ambient temperature on a Bruker E500 spectrometer.

### 2.3. Desulfurization testing

The model oil was prepared by dissolving BT, or DBT, or 4,6-DMDBT in *n*-decane with a corresponding S-content of 500 ppm.

Desulfurization of the model oil was carried out in a homemade photocatalytic reactor equipped with a high pressure mercury lamp (100 W, with a main peak at 365 nm), as shown in Fig. S1 in the supporting information (SI). According to the specific reaction conditions, 15 mL of model oil, a certain amount of GO, MeA, MeCN, and air were mixed in the quartz flask with magnetic stirring. 50  $\mu$ L of the oil samples were periodically removed and further analyzed using gas chromatography flame ionization detection (GC-FID) (GC9800, Shanghai Kechuang Chromatograph Instrument Co., Ltd., SE-54 column,  $l$  15 m  $\times$   $\Phi$  0.53 mm  $\times$  1.0  $\mu$ m) by adding tetradecane as an internal standard. The chromatographic procedure were as follows: injection volume of 0.2  $\mu$ L, inlet temperature of 250  $^{\circ}$ C, detector temperature of 270  $^{\circ}$ C, column temperature of 120  $^{\circ}$ C heated to 165  $^{\circ}$ C (with 10  $^{\circ}$ C min $^{-1}$  increases), holding at 165  $^{\circ}$ C for 1 min then heating to 220  $^{\circ}$ C (with 20  $^{\circ}$ C min $^{-1}$  increases), and holding at 220  $^{\circ}$ C for 4 min. Sulfur removal was used to indicate the conversion of sulfur compounds, which was calculated by the following Eq. (1):

$$\text{Sulfur removal} = (C_1 - C_2)/C_1 \times 100\% \quad (1)$$

where  $C_1$  and  $C_2$  were respectively the initial and residual sulfur contents of the model oil.

#### 2.4. Computational details

DFT is a popular method for explaining molecular reactivity because of its good compromise between accuracy and computational efficiency. DFT calculations were carried out with the Coulomb attenuating method CAM-B3LYP hybrid functional [46] or M062X [47] using the 6-311+G(d,p) basis set, as implemented in the Gaussian 09 software package [48]. Solvent effects in MeCN were assessed using the polarizable continuum model (PCM) [49]. The electronic energies and charges based on natural population analysis (NPA) were calculated using unrestricted UCAM-B3LYP. The restricted open-shell ROCAM-B3LYP approach was used to predict the frontier molecular orbitals of the open-shell systems, including  $^3\text{O}_2$ ,  $\text{HO}^{\bullet}$ ,  $\text{O}_2^{\bullet-}$ ,  $\text{HO}_2^{\bullet-}$ , and the lowest-lying triplet state ( $T_1$ ) of each of BT, DBT, and 4,6-DMDBT. The electronic absorption spectra of BT, DBT, and 4,6-DMDBT in MeCN were simulated to rationalize their basic photocatalytic behaviour, using time-dependent density functional theory (TDDFT) [50] at the CAM-B3LYP/6-311+G(d,p) level. The energy barriers among GO,  $\text{O}_2$ , and the active intermediate at the M062X/6-311+G(d,p) level of theory were computed and show promising excellent results for calculating the interaction energies [51].

### 3. Results and discussion

#### 3.1. DBT removal in different reaction systems

Fig. 1 depicts the removal of DBT from model oil in different reaction systems. Sulfur removal was very low under the reaction condition of only MeCN (24.7%) and only UV radiation (11.7%) with air as the oxidant. With adding MeA or GO to the model oil under UV radiation, sulfur removal reached 72.3% or 93.6% (S content >25 ppm), respectively, in 140 min, but the approach still failed to reach deep desulfurization [52]. However, when GO and MeA were simultaneously added to the abovementioned system and formed EPODS, sulfur removal increased significantly, reaching 99.9% (S content <10 ppm) and achieving deep desulfurization. When MeCN was absent from the system, sulfur removal decreased sharply to 51.3%. This was reasonable because hydrophilic GO exhibited poor dispersibility in the oil phase compared to that in MeCN, which inhibited the catalytic activity of GO. Notably, sulfur removal was still quite high (94.1%) in the system with no air-bubbling. This was mainly due to the high solubility of  $\text{O}_2$  in MeCN at 25  $^{\circ}$ C

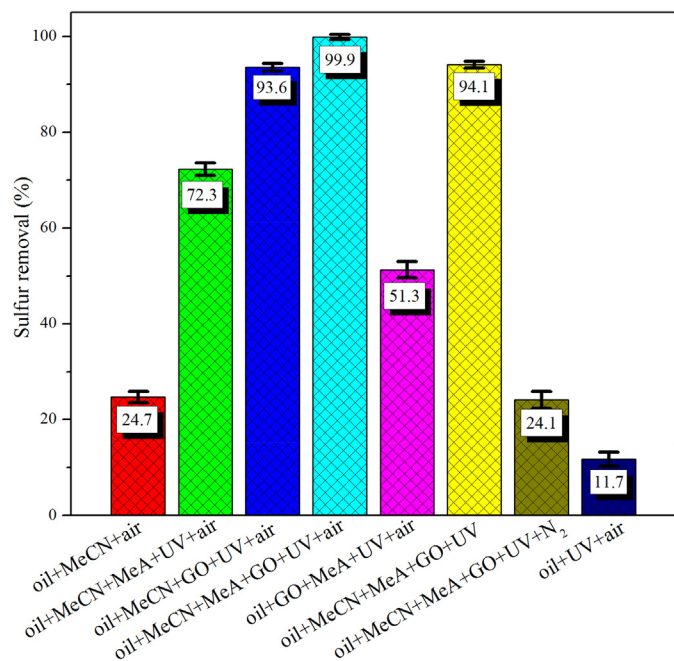


**Fig. 1.** DBT removal from model oil using different photocatalytic desulfurization systems. Experiment conditions:  $T=25^{\circ}\text{C}$ ,  $m(\text{GO})=0.6\text{ mg}$ ,  $V(\text{model oil})=15\text{ mL}$ ,  $V(\text{MeCN})=7.5\text{ mL}$ ,  $V(\text{MeA})=4.5\text{ mL}$ ,  $t=140\text{ min}$ , and  $v(\text{air})=20\text{ mL min}^{-1}$ .

(8 mmol L $^{-1}$ ) [53,54], which led to the inevitable dissolution of  $\text{O}_2$  in MeCN in the presence of air. When air-bubbling was replaced by  $\text{N}_2$ -bubbling in the abovementioned EPODS, sulfur removal dramatically decreased to 24.1%. Overall, these results indicate that GO and MeA form a photocatalytic system, promoting the conversion of DBT into the oxidized product with air under UV radiation. Thus, both MeCN as the extractant and  $\text{O}_2$  as the oxidant play important roles in the desulfurization reaction process.

#### 3.2. Effects of reaction conditions on sulfur removal

Fig. 2a shows the effect of the amount of GO on the removal of DBT. Sulfur removal increased with an increasing amount of GO from 0.2 mg to 0.6 mg and reached a maximum of 99.9% in 140 min. A further increase in the amount of GO led to a reduction in sulfur removal. This is reasonable because the introduction of black GO can lead to a significant increase in the opacity of the MeCN phase, which reduces the light absorption by the reaction system. At 140 min, sulfur removal from the system with 0.4 and 0.6 mg GO were 99.5% (S content = 2.5 ppm) and 99.9% (S content = 0.5 ppm), respectively, both of which reached the requirements for deep desulfurization (S content <10 ppm) in transportation fuels. However, 0.6 mg GO exhibited a slightly higher desulfurization effect, which may provide an available reference for ultraclean fuel (S content <1 ppm) as a potential feedstock for fuel-cell applications [53,55]. Therefore, 0.6 mg GO was chosen as the most suitable amount in the following investigation, and this was an ultra-low catalyst dosage compared with other metal-containing photocatalysts [32,34,56].

Fig. 2b shows the effect of  $r_{\text{M}/\text{o}}$  on the removal of DBT. It is clear that the reaction temperature had a significant influence on the removal of DBT. When  $r_{\text{M}/\text{o}}$  was increased from 1:8 to 1:2, a remarkable increase in the removal of DBT was observed. At 1:8, only 57% of the DBT was removed from the model oil, while at 1:2 almost all of the DBT was removed within 140 min. Interestingly, continuing to increase  $r_{\text{M}/\text{o}}$  to 1:1.5, resulted in almost no more increase in the removal of DBT. The above results implied that the increase in the

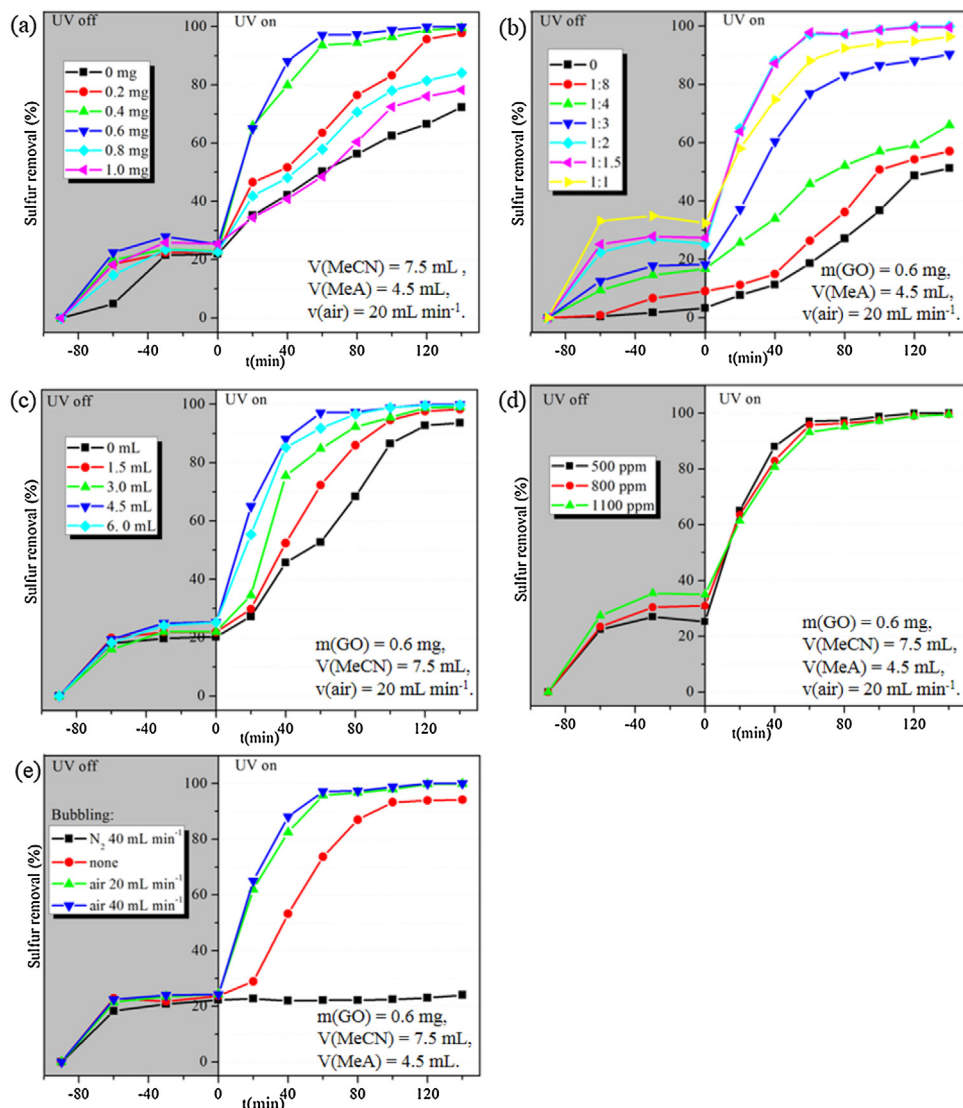


**Fig. 2.** Effects on the removal of DBT by (a) the amount of GO, (b) the  $r_{M/o}$ , (c) the amount of MeA, (d) the initial S-concentration, and (e) air/ $N_2$  bubbling. Other identical experimental conditions:  $T = 25^\circ\text{C}$  and  $V(\text{model oil}) = 15 \text{ mL}$ .

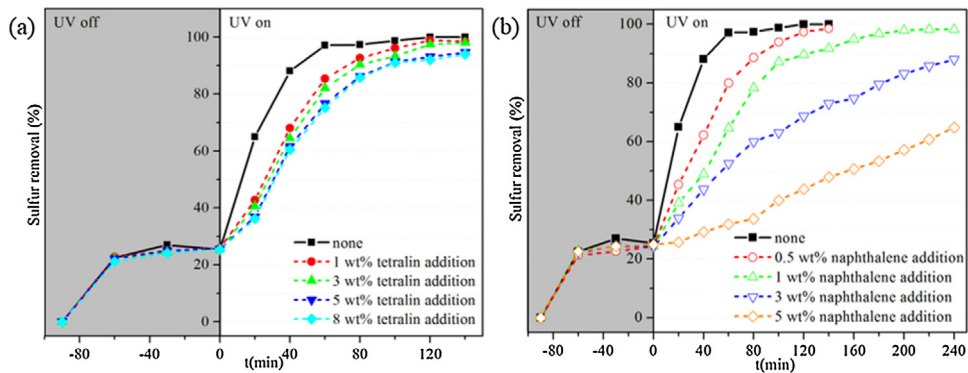
amount of MeCN improved the mass transfer effect between the oil and the extraction phases. High sulfur removal can be obtained by using the proper amount of MeCN. However, too much MeCN may dilute the concentration of the ROS produced by UV irradiation, instead of reducing the reaction rate. It was further confirmed that a decline in sulfur removal was observed when  $r_{M/o}$  was 1:1.

Fig. 2c shows the effect of the amount of MeA on the removal of DBT. It was observed that a relatively high sulfur removal (93.6%) was achieved in the absence of MeA. An increase in the amount of MeA from 1.5 mL to 4.5 mL slightly increased the amount of sulfur removal. However, a further increase in the amount of MeA (6 mL) did not continue to improve sulfur removal. This implied that MeA was not a decisive factor but only plays a role in stabilizing the ROS in the photocatalytic desulfurization process.

The initial concentration of sulfur compounds cannot be neglected in considering the deep desulfurization of various oils in practical processes. Fig. 2d shows the effect of the initial DBT concentration on sulfur removal. The sulfur removal decreased very slightly when the initial concentration of DBT was increased from 500 ppm to 1100 ppm. In particular, the sulfur removal still reached 99.5% in 140 min with a high initial S-concentration of 1100 ppm,

which was difficult to achieve in the  $\text{TiO}_2$  photocatalytic desulfurization system [10]. Also, the high amount of sulfur removal achieved in current reaction system with a high initial DBT concentration was slightly better than that of photochemical ODS with isobutylaldehyde [35]. Thus, this may provide a potential technology for the deep desulfurization for high S-content oils.

Fig. 2e shows the effect of air/ $N_2$  bubbling on the removal of DBT. Sulfur removal was dramatically facilitated by the bubbling of air or  $O_2$  but was suppressed by  $N_2$  bubbling. At a  $N_2$  flow rate of  $40 \text{ mL min}^{-1}$ , the sulfur removal of DBT sharply decreased to 24%, indicating that DBT could not be oxidized and was only extracted by MeCN. In the case of no air bubbling, the sulfur removal was still as high as 94.1%, and this was mainly attributed to the dissolved  $O_2$  in MeCN. An increase in the air flow rate from  $20 \text{ mL min}^{-1}$  to  $40 \text{ mL min}^{-1}$  caused almost no increase in the sulfur removal because of the introduction of sufficient  $O_2$  into the reaction system at a lower air inflow rate. These observations demonstrated that  $O_2$  plays a vital role in further formation of ROS to oxidize sulfur compounds, and this is consistent with the observed results reported in other aerobic ODS systems [35,57,58].



**Fig. 3.** Effects of the amount of tetralin (a) and naphthalene (b) on sulfur removal from model oil. Experiment conditions:  $T=25^{\circ}\text{C}$ ,  $V(\text{model oil})=15 \text{ mL}$ ,  $m(\text{GO})=0.6 \text{ mg}$ ,  $V(\text{MeCN})=7.5 \text{ mL}$ ,  $V(\text{MeA})=4.5 \text{ mL}$ , and  $v(\text{air})=20 \text{ mL min}^{-1}$ .

### 3.3. Effects of additional aromatic compounds on sulfur removal

Real oil contains a certain amount of aromatic hydrocarbons, consisting of mono-, di-, and polycyclic aromatics that depress the photochemical reaction of HASCs [59,60]. Here, tetralin and naphthalene were chosen as representative mono- and dicyclic aromatics to investigate their effects on the removal of DBT because the content of polycyclic aromatics in diesel fuel is strictly limited according to China V diesel fuel quality standards. As shown in Fig. 3a, the sulfur removal after 140 min of reaction was 98.4%, 98.0%, 94.7%, and 93.9% with the addition of 1 wt%, 3 wt%, 5 wt%, and 8 wt% tetralin, respectively. Sulfur removal decreased slightly with an increasing concentration of tetralin. As shown in Fig. 3b, the sulfur removal after 140 min of reaction was 98.5%, 91.7%, 72.9%, and 47.8% with the addition of 0.5 wt%, 1 wt%, 3 wt%, and 5 wt% naphthalene, respectively. Compared to the tetralin addition, sulfur removal decreased remarkably with an increasing concentration of naphthalene. This is because a triplet-energy transfer from the photoexcited DBT to the ground-state naphthalene occurred [60]. Consequently, the photooxidation of DBT was suppressed more strongly by naphthalene. Although prolonging the reaction time further, did slowly increase the final sulfur removal with the successive photodecomposition of naphthalene, it was a time-consuming and energy-consuming measure. Therefore, bicyclic aromatics should be separated prior to UV irradiation based on the current method to achieve efficient deep desulfurization.

### 3.4. Recycling of the reaction system for EPODS

The recycling experiments of EPODS were conducted using DBT as the substrate. The results are shown in Fig. 4. After reaction, the upper oil was separated from the reaction system by static layering. Fresh model oil containing DBT was added to the lower phase containing the GO, MeA, and MeCN for the next cycle. After the reaction system was recycled three times, the sulfur removal remained 97.7%. For the fourth and fifth cycles, the sulfur removal decreased to 77.9% and 55.1%, respectively. The sharp decrease in the desulfurization activity may be caused by oxygenated DBT, which was absorbed by GO and decreased the active sites. Meanwhile, excessive oxidized products in MeCN also inhibited the reaction rate of DBT. It is very important to remove oxidized products from MeCN after reaction using appropriate methods, such as distillation. The change of oxygen-containing functional groups in GO was also an important reason for the decrease in sulfur removal, and this was confirmed by XPS, ATR FT-IR, and Raman characterizations which are discussed in the next section.

### 3.5. Characterization of fresh and spent GO

As described in the *Introduction*, the exact structure and composition of GO remains a challenge in chemical reactions. Hence, the morphological and active site changes of fresh GO (before reaction) and spent GO (after reaction) were focused on in this work to help

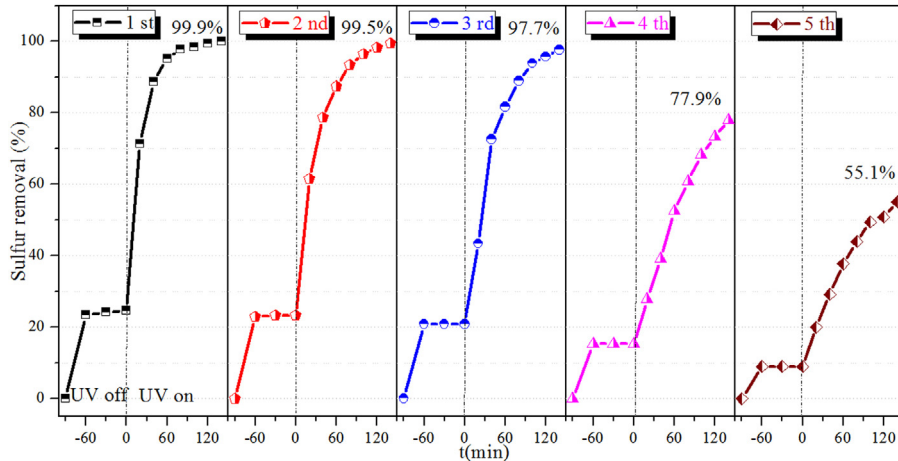


**Fig. 4.** Recycling of GO and MeCN for EPODS. Experiment conditions:  $T=25^{\circ}\text{C}$ ,  $V(\text{model oil})=15 \text{ mL}$ ,  $m(\text{GO})=0.6 \text{ mg}$ ,  $V(\text{MeCN})=7.5 \text{ mL}$ ,  $V(\text{MeA})=4.5 \text{ mL}$ , and  $v(\text{air})=20 \text{ mL min}^{-1}$ .

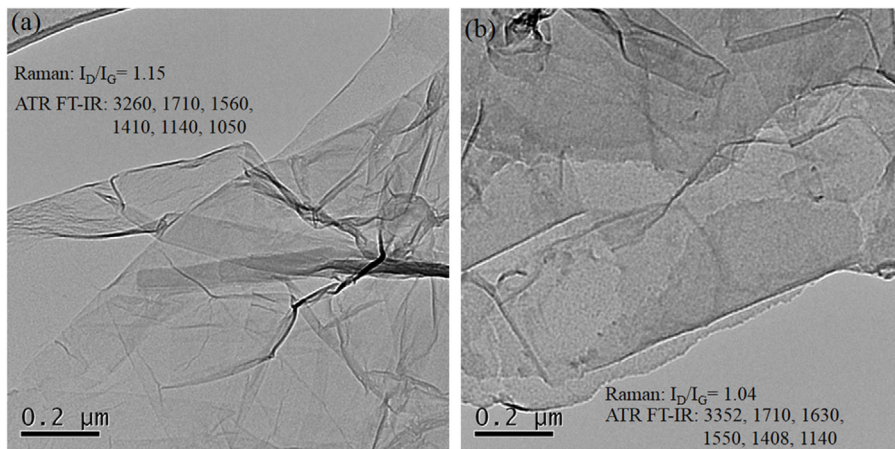


**Fig. 5.** TEM images of (a) fresh and (b) spent GO samples. The inset values represent the  $I_D/I_G$  ratios and the wavenumbers of some characteristic peaks obtained from Raman and ATR FT-IR spectra, respectively, for each sample. (See Fig. S2 and S3 in SI.).

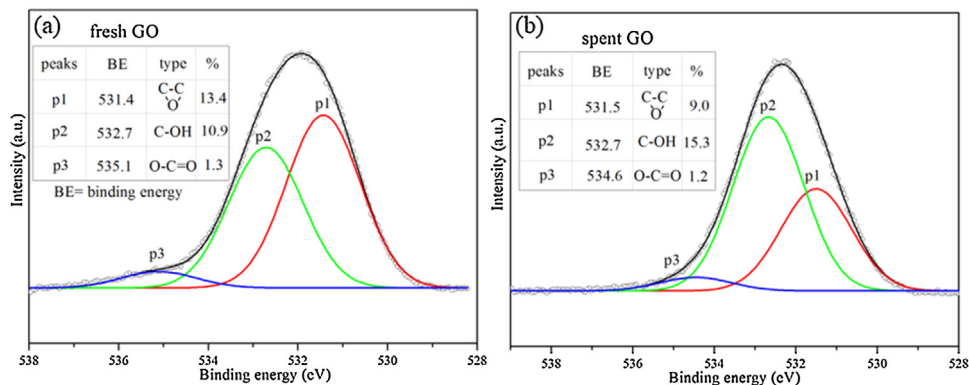


**Fig. 6.** High-resolution XPS O1s spectra obtained for (a) fresh and (b) spent GO samples.

further analyze the mechanism of the desulfurization reaction. The TEM images (Fig. 5a) showed that fresh GO had an apparent flaky morphology. After the desulfurization reaction, the flaky morphology of GO was well preserved without noticeable changes, as shown in Fig. 5b. However, scattered stain spots were observed in the spent GO due to the adsorption of oxidation products, and this led to its declining catalytic performance. The Raman spectrum (Fig. S2 in SI) displayed a decrease in the intensity of the D band compared to that of the G band, indicating a substantial increase in  $sp^2$ -bonded carbon atoms and oxidized molecular defects [61]. This shows that the desulfurization process alters the structure of GO and specifically introduces structural defects. Fig. S3 in SI shows the ATR FT-IR spectra for fresh and spent GO. The spectrum of fresh GO displays bands at 1710( $\nu_{C=O}$ ) cm<sup>-1</sup>, 1560( $\nu_{as,O-C=O}$ ) cm<sup>-1</sup>, 1410( $\nu_{s,O-C=O}$ ) cm<sup>-1</sup>, 1140( $\nu_{C-O-C}$ ) cm<sup>-1</sup>, 1050( $\nu_{C-O}$ ) cm<sup>-1</sup>, and a broad band at 3260( $\nu_{O-H}$ ) cm<sup>-1</sup> due to the intramolecular H-bonds present on GO. After reaction, the intensities of the peaks at 1560 cm<sup>-1</sup>, 1410 cm<sup>-1</sup>, and 1140 cm<sup>-1</sup> were lower, suggesting that the O-C=O, C-O-C, and C-OH groups participated in the reaction.

Further, the detailed nature of the oxygen-containing functional groups in GO were confirmed by XPS. The XPS survey (Fig. S4 in SI) shows that the ratio of C/O in fresh and spent GO was 2.92 and 3.12, respectively, suggesting trace amounts of oxygen-functional groups were lost during the desulfurization process. The high-resolution O1s spectra (Fig. 6) can be deconvoluted into several components, including epoxy oxygen (C-O-C), in-plane central pyran-type oxygen (C-O), hydroxyl oxygen (C-OH), and edge carbonyl oxygen (C=O), and this is in agreement with the reported literature [45]. Compared to fresh GO, the peak intensi-

ties of the epoxy oxygen in the spent GO decreased (from 13.4% to 9.0%) while C-O(H) increased (from 10.9% to 15.3%), and this was also confirmed by high-resolution C1s spectra (Fig. S5 in SI). These observations also indicate that the repeated use of GO led to the decrease in sulfur removal, which may have been caused by the reduction of epoxy groups. In Section 3.7, the DFT results provide a more detailed explanation of the role of oxygen-containing functional groups in GO.

### 3.6. Oxidation reactivities of different sulfur compounds

It is well known that BT and DBT account for more than 50% of the total sulfur in diesel fuel, whereas the largest fraction of HASCs present in low-sulfur diesel fuels are C2-DBTs such as 4,6-DMDBT [62]. Consequently, investigating the oxidation reactivities of HASCs is important for designing the reaction process in industrial applications. Fig. 7 shows the reactivities of BT, DBT, and 4,6-DMDBT. The sulfur removals of BT, DBT, and 4,6-DMDBT reached 100% (in 100 min), 99.9% (in 140 min), and 99.4% (in 140 min), respectively, indicating that the reactivities of these HASCs followed the order: BT > DBT > 4,6-DMDBT. It has been reported that the reactivities of HASCs have different orders under specific reaction conditions. As reported by Otsuki et al. [63], generally, the reactivities of HASCs improve with an increase in the electron density at the sulfur atom in each BT, DBT, and 4,6-DMDBT, which are 5.739, 5.758, and 5.760, respectively. Specifically, the reactivities of HASCs decrease in the order of 4,6-DMDBT > DBT > BT, and this has been observed frequently in the extraction and thermocatalytic ODS systems [58,64]. Subsequently,

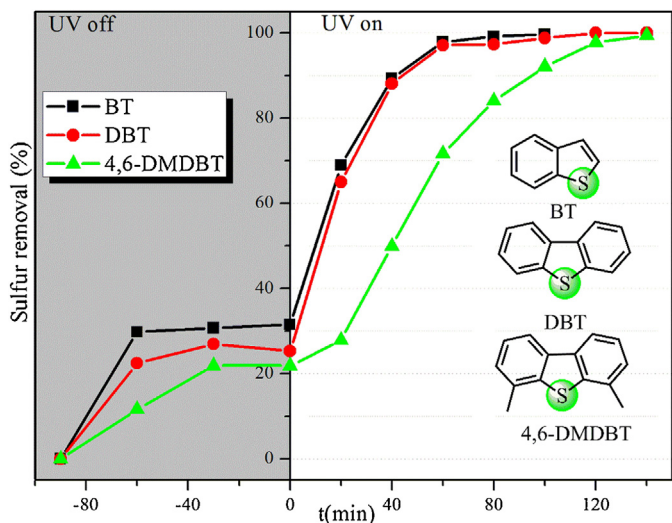


**Fig. 7.** Effects of different substrates on sulfur removal. Experiment conditions:  $T = 25^\circ\text{C}$ ,  $V(\text{model oil}) = 15 \text{ mL}$ ,  $m(\text{GO}) = 0.6 \text{ mg}$ ,  $V(\text{MeCN}) = 7.5 \text{ mL}$ ,  $V(\text{MeA}) = 4.5 \text{ mL}$ , and  $v(\text{air}) = 20 \text{ mL min}^{-1}$ .

**Table 1**

Natural charges and natural populations of sulfur atoms in HASCs using UCAM-B3LYP/6–311+G(d,p) in MeCN.

State	HASCs	Natural charge	Natural population			
			Core	Valence	Rydberg	total
$S_0$	BT	0.375	9.999	5.581	0.046	15.626
	DBT	0.371	9.999	5.592	0.039	15.629
	4,6-DMDBT	0.353	9.999	5.608	0.041	15.647
$T_1$	BT	0.324	9.999	5.626	0.051	15.676
	DBT	0.701	9.999	5.258	0.042	15.299
	4,6-DMDBT	0.660	9.999	5.300	0.041	15.340

with the continuous development of ODS research, more often the trends of DBT > BT > 4,6-DMDBT [65–67] or DBT > 4,6-DMDBT > BT [68–70] have been reported. These reactive trends of HASCs can be reasonably explained by electron density and steric hindrance arguments. However, in some rare cases, the reactivities of HASCs decrease in the order of BT > DBT > 4,6-DMDBT [35,71], which is the complete reverse relative to the order of sulfur electron densities. Zhu et al. [35] proposed that this might be mainly because the steric hindrance in HASCs becomes a major factor in the presence of big active oxygen species (such as peroxy isobutyrate). There remain some uncertainties, however, because BT and DBT possess almost the same amount of steric effects while the reactivity of BT, which has a lower electron density at its S atom, had a higher reactivity than that of DBT.

In previous theoretical investigations [63,72], the electron densities of S atoms in different HASCs were obtained using the semi-empirical quantum mechanical method (SQM). However, SQM only supplies limited information for molecular reactivities due to the valence-only  $sp$  basis sets and the neglect of differential overlap [73]. Extensive research suggested that DFT analysis can provide useful insights into the photocatalytic properties of compounds [74]. Here, DFT calculations were employed to establish a basis for the detailed knowledge of the current photocatalytic reactions of BT, DBT, and 4,6-DMDBT, with the aim of revealing the origin of the differences in their reactivities under UV radiation.

NPA calculations can be used to gain deeper insights into the electronic structures of HASCs and their affinities for ROS [75]. As given in Table 1, the valence electrons of the sulfur atoms for ground state BT( $S_0$ ), DBT( $S_0$ ), and 4,6-DMDBT( $S_0$ ) are 5.581, 5.592, and 5.608, respectively, and these are close to the electron den-

**Table 2**  
Energies (in eV) of some FMOs for HASCs computed using ROCAM-B3LYP/6–311+G(d,p) in MeCN.

State	FMO	BT	DBT	4,6-DMDBT
$S_0$	HOMO-1	-8.182	-7.823	-7.725
	HOMO	-7.630	-7.537	-7.438
	LUMO	0.102	-0.283	-0.191
	LUMO + 1	0.616	0.492	0.680
$T_1$	SOMO-1	-3.725	-3.870	-3.822
	SOMO	-1.324	-1.529	-1.477
	LUMO	0.635	0.533	0.734
	LUMO + 1	0.811	0.785	0.777

sities reported by Otsuki et al. [63]. Also, atomic natural charges have frequently been used to describe molecular reactivities. From an electrostatic point of view, we agree that 0.4 GO is enough higher electropositive atoms have a lower ability to donate electrons. The natural charges of sulfur atoms for BT( $S_0$ ), DBT( $S_0$ ), and 4,6-DMDBT( $S_0$ ) are 0.375, 0.371, and 0.353, respectively, indicating that the oxidation reactivities increase. Furthermore, frontier molecular orbital (FMO) theory [76] determined by the highest-unoccupied molecular orbital (HOMO) and the lowest-unoccupied molecular orbital (LUMO), is useful in a wide range of reactivity problems. As given in Table 2, the energies of HOMOs of BT( $S_0$ ), DBT( $S_0$ ), and 4,6-DMDBT( $S_0$ ) were -7.630 eV, -7.537 eV, and -7.438 eV, respectively, suggesting that their abilities to provide electrons increase in that sequence.

Overall, the aforementioned electronic structures of BT, DBT, and 4,6-DMDBT, each in the  $S_0$  state, indicated that their oxidation reactivities increase in this order, and this is in good agreement with previous theoretical and experimental observations [58,63,64,72]. However, the reported theoretical results based on the  $S_0$  state were the complete opposite of both the experimental reactivities of HASCs available in the literature [35] and the current observations made under UV radiation. To gain insight into the unusual phenomenon regarding these EPODS systems, the excited state properties of HASCs were considered using TDDFT. According to the computed absorption-spectral wavelengths of BT, DBT, and 4,6-DMDBT given in Fig. S6a-c in SI, HASCs absorb photons and transition from the ground state to the excited state. Generally, the first excited singlet ( $S_1$ ) and the  $T_1$  state are the most important electronically excited states for photochemical properties of molecules. Here, only the  $T_1$  state was considered for further analysis of the HASCs reactivities because it is energetically preferred over the  $S_1$  state.

As displayed in Tables 1 and 2, BT( $T_1$ ) had the lowest natural charge (0.324) for the S atom, the highest valence electron (5.626), and the highest singly occupied molecular orbital (SOMO) energy (-1.324 eV), all of which indicate that it would exhibit the best reactivity for oxidation in the  $T_1$  state. Similarly, 4,6-DMDBT( $T_1$ ) should have better reactivity for oxidation than DBT( $T_1$ ) depending on the relationship of the electronic structures. However, since 4,6-DMDBT had two methyl groups, leading to large steric hindrance, it exhibited the lowest reactivity for oxidation. Under UV radiation, therefore, these observations indicate that HASCs reactivities were dominated by their electronic structures of the  $T_1$  states and steric hindrance, rather than the  $S_0$  states.

In addition, the interaction of ground-state oxygen ( $^3\text{O}_2$ ) with HASC( $S_1$ )\* were investigated at the CAM-B3LYP/6–311+G(d,p) level in MeCN. One possible channel is through the energy transfer process as shown in Eq. (2). This is an exothermic reaction with an enthalpy change of  $\Delta H = -\Delta E_{ST} + 22.4 \text{ kcal mol}^{-1}$ , where  $\Delta E_{ST}$  is the energy difference between HASC( $S_1$ )\* and HASC( $T_1$ )\*, and 22.4 kcal mol $^{-1}$  is the energy required to generate  $^1\text{O}_2$ \*. When  $\Delta E_{ST}$  is greater than 22.4 kcal mol $^{-1}$ , the energy transfer process of Eq. (2) can occur from an energy point of view. As shown in Fig. 8,  $\Delta E_{ST}$

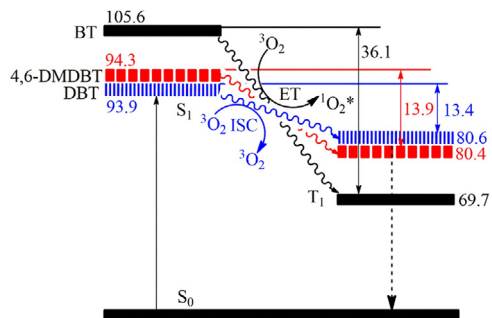


**Fig. 8.** Relative energies (in  $\text{kcal mol}^{-1}$ ) of excited states using CAM-B3LYP/6-311+G(d,p) in MeCN. ET: Energy transfer and ISC: Intersystem crossing.

for BT, DBT, and 4,6-DMDBT are 36.1 kcal mol<sup>-1</sup>, 13.4 kcal mol<sup>-1</sup>, and 13.9 kcal mol<sup>-1</sup>, respectively, indicating that only BT(S<sub>1</sub>)<sup>\*</sup> can interact with <sup>3</sup>O<sub>2</sub> through energy transfer to yield <sup>1</sup>O<sub>2</sub><sup>\*</sup>. Subsequently, <sup>1</sup>O<sub>2</sub><sup>\*</sup> is not only a more powerful oxidant than <sup>3</sup>O<sub>2</sub>, but can also further react with hydrocarbons or H<sub>2</sub>O to yield HO<sup>•</sup>. However, DBT(S<sub>1</sub>)<sup>\*</sup> and 4,6-DMDBT(S<sub>1</sub>)<sup>\*</sup> transformed to DBT(T<sub>1</sub>)<sup>\*</sup> and 4,6-DMDBT(T<sub>1</sub>)<sup>\*</sup>, respectively, through spin-catalysis of <sup>3</sup>O<sub>2</sub> and intersystem crossing (ISC) as shown in Eq. (3). Thus, BT can react with more ROS than DBT and 4,6-DMDBT, which is consistent with its observed highest reactivity.

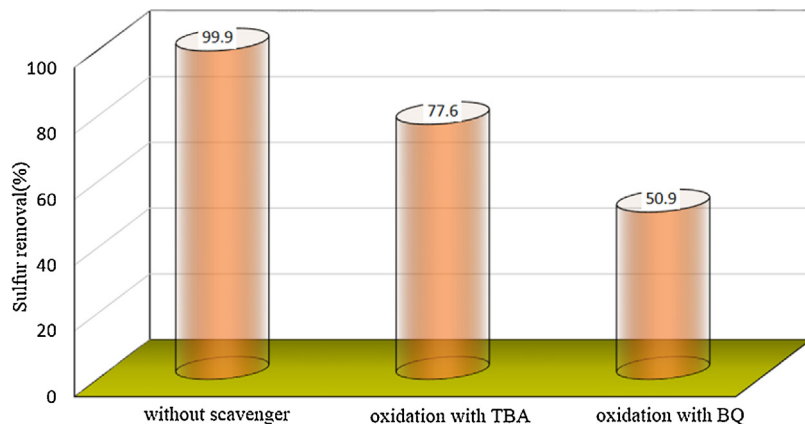
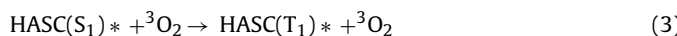
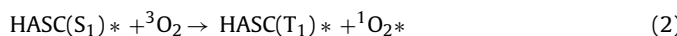


**Fig. 9.** Effects of scavengers on the removal of DBT. Experiment conditions:  $T = 25^\circ\text{C}$ ,  $V(\text{model oil}) = 15 \text{ mL}$ ,  $m(\text{GO}) = 0.6 \text{ mg}$ ,  $V(\text{MeCN}) = 7.5 \text{ mL}$ ,  $V(\text{MeA}) = 4.5 \text{ mL}$ ,  $v(\text{air}) = 20 \text{ mL min}^{-1}$ ,  $c(\text{TBA}) = 20 \text{ mM}$ , and  $c(\text{BQ}) = 20 \text{ mM}$ .

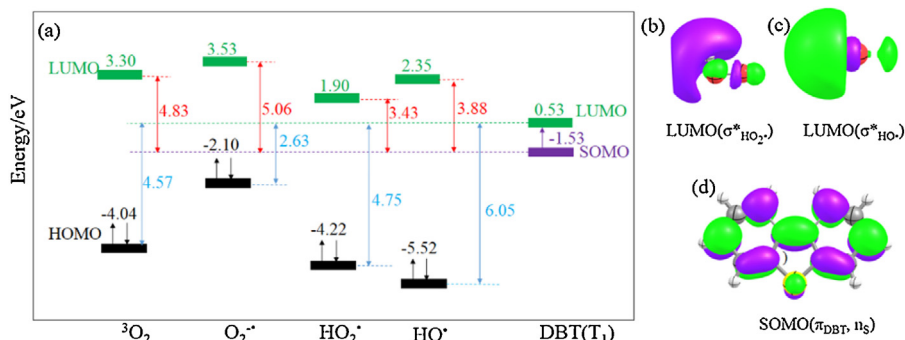


**Fig. 10.** (a) Energies of the HOMOs (or SOMO) and the LUMOs of ROS and DBT. The LUMO isosurfaces of (b)  $\text{HO}_2^*$  and (c)  $\text{HO}^*$ . (d) The SOMO isosurface of DBT.

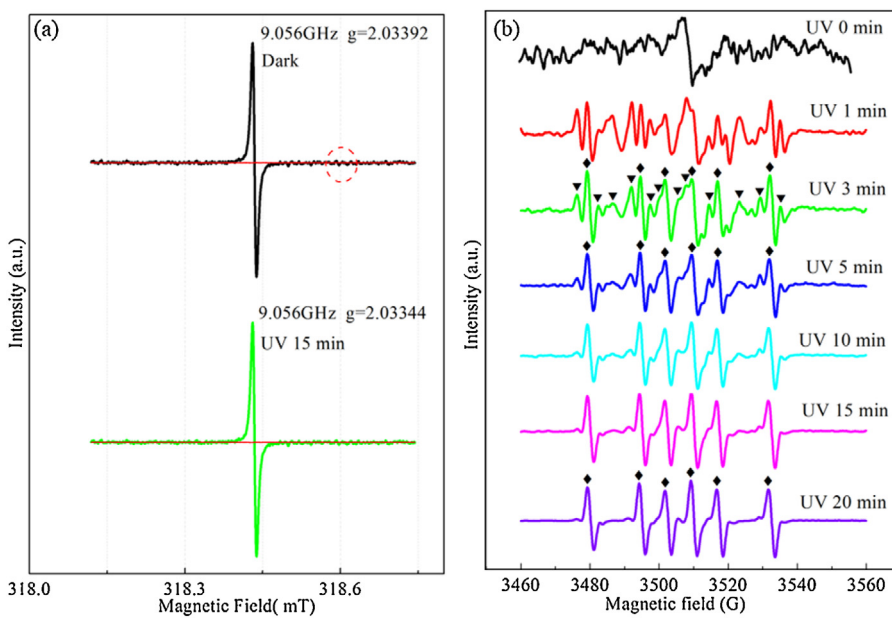


Fig. 11. ESR spectra (a) without DMPO and (b) with DMPO for the reaction system in situ under UV radiation.

respectively, indicating that it is very difficult for  ${}^3\text{O}_2$  and  $\text{O}_2\cdot^-$  to be involved in the oxidation reaction of DBT in the presence of  $\text{HO}_2^{\cdot}$  and  $\text{HO}^{\cdot}$ . Notably, the relatively high value of  $E(\text{HOMOO}_2^{\cdot-})$ , which is  $-2.10\text{ eV}$ , indicates that  $\text{O}_2\cdot^-$  itself was a good reducing agent, rather than a good oxidizer.

Fig. 10b–d shows the LUMO isosurfaces of  $\text{HO}_2^{\cdot}$  and  $\text{HO}^{\cdot}$  and the SOMO isosurface of DBT. The LUMO isosurfaces of  $\text{HO}_2^{\cdot}$  and  $\text{HO}^{\cdot}$  were each predominantly an antibonding  $\sigma$  orbital ( $\sigma^*$ ) over the whole radical, while the SOMO isosurface of DBT was largely delocalized  $\pi$  orbitals ( $\pi_{\text{DBT}}$ ) of the aromatic ring and a nonbonding orbital of the S atom ( $n_{\text{S}}$ ). Hence, these areas were expected to be the active sites of the reaction.

However, how to generate  $\text{HO}_2^{\cdot}$  and  $\text{HO}^{\cdot}$  and the initial step of the reaction are still ambiguous. To directly observe the signals of the radicals, the ESR measurement was performed in situ under UV radiation. As shown in Fig. 11a, the reaction system displayed a sharp and intensive resonance peak with  $g = 2.034$ , which was attributed to the excessive  $\pi$ -electrons in the GO edges [80,81], while the imperceptible ESR signal in the red circle may originate from the adsorbed  ${}^3\text{O}_2$  over the GO nanosheet edges [81]. The absence of any free radicals was observed in the reaction system without introducing other agents, possibly because of the short lifetimes of the free radicals. After the spin-trapping agent 5,5-dimethyl-1-pyrroline-N-oxide (DMPO) was added to the reaction system, a complex ESR signal consisting of a sixfold peak ( $\blacklozenge$ ) and a twelvefold peak ( $\blacktriangledown$ ) was detected within 3 min of UV irradiation. This is displayed in Fig. 11b and is similar to the signals of the carbon radical generated by isobutyraldehyde [35]. The sixfold peak was a typical DMPO- $\text{R}^{\cdot}$  or DMPO- $\text{RO}^{\cdot}$  signal, which corresponded to  $\text{GO}^{\cdot}$  and  $\text{GO}-\text{C}(\text{O})^{\cdot}$  (indicating the spin electron in the C atom) radicals produced from GO under UV radiation. The twelvefold peak was attributed to DMPO-GO- $\text{C}(\text{OOO})^{\cdot}$  formed by  $\text{GO}-\text{C}(\text{O})^{\cdot}$  and adsorbed  ${}^3\text{O}_2$ . Unlike most reports [32,33,82], neither  $\text{HO}_2^{\cdot}$  nor  $\text{HO}^{\cdot}$  characteristic ESR signals were observed. This is because the signals of radical adducts for DMPO- $\text{O}_2^{\cdot-}$  (or  $\text{HO}_2^{\cdot}$ ) and DMPO- $\text{HO}^{\cdot}$  are usually observed in methanol and water, respectively, in ESR measurements [83]. To maintain the original situation of the current system, neither methanol nor water was added for the ESR test. Notably, the peaks corresponding to DMPO-GO- $\text{C}(\text{OOO})^{\cdot}$  gradually disappeared, leaving only the clear sixfold peaks of DMPO-GO-

or DMPO-GO $^{\cdot}$  after 15 min of UV irradiation. This implied that  $\text{GO}-\text{C}(\text{OOO})^{\cdot}$  transformed to more stable non-radical forms, such as  $\text{GO}-\text{COOOH}$ . Consequently, it was imperative to examine further the formation of  $\text{GO}^{\cdot}$  and  $\text{GO}-\text{C}(\text{O})^{\cdot}$  to gain a thorough understanding of the mechanism.

The mechanism for the generation of  $\text{GO}^{\cdot}$ ,  $\text{GO}-\text{C}(\text{O})^{\cdot}$ ,  $\text{GO}-\text{COOO}^{\cdot}$ , and other possible forms was investigated using DFT at the M062X/6-311+G(d,p) level, which gives reasonable results for calculating the interaction energies of neutral and radical reactions [51]. As shown in Fig. S7a, the potential active sites in GO proposed by Su et al. include armchair edge, zigzag edge, and defect sites [42], where the epoxy, hydroxyl, and carboxyl groups as well as the spin electrons are found. To simplify the computations, herein representative sites were considered as including the in-plane epoxy group at the armchair edge ( $\text{GO}_a>\text{O}$ , Fig. S7b) [84], the hydroxyl group at the zigzag edge ( $\text{GO}_z-\text{OH}$ , Fig. S7c) and the defect site ( $\text{GO}_d-\text{OH}$ , Fig. S7d), and the carboxyl group at the zigzag edge ( $\text{GO}_z-\text{COOH}$ , Fig. S7e) and the defect site ( $\text{GO}_d-\text{COOH}$ , Fig. S7f). Corresponding to the oxygen-containing groups located at different active sites, three reaction paths are proposed in Fig. 12.

In path I (Fig. 12a),  $\text{GO}_a>\text{O}$  first transitioned from  $S_0$  to the  $S_1$  state with an excitation energy of  $58.4\text{ kcal mol}^{-1}$  under UV radiation, and then transformed to the  $T_1$  state by ISC (omitting the energy transfer mode here) with an releasing energy of  $25.9\text{ kcal mol}^{-1}$ . At the  $T_1$  state,  $\text{GO}_a>\text{O}$  forms the biradical ( $\text{GO}_a^{\cdot}-\text{O}^{\cdot}$ ) through C–O cleavage overcoming a low energy barrier of  $10.2\text{ kcal mol}^{-1}$ , indicating that this process occurred easily.  $\text{GO}_a^{\cdot}-\text{O}^{\cdot}$  or  $\text{GO}_a(\text{O}_2)^{\cdot}-\text{O}^{\cdot}$  generated with  ${}^3\text{O}_2$  might be captured by DMPO to form an adduct DMPO-GO- $\text{C}(\text{OOO})^{\cdot}$ , which is in good agreement with the observed complex ESR signal at the beginning of UV irradiation.  $\text{GO}_a^{\cdot}-\text{O}^{\cdot}$  is a lively biradical, and thus it can preferentially form stable intermediates with the ambient  $\text{H}^+$  and additional electrons (proton-electron pair) around the absorbed  $\text{O}_2$  on GO. Channel A is:  $\text{GO}_a^{\cdot}-\text{O}^{\cdot} + 2\text{H}^+ + 2\text{e}^- \rightarrow \text{GO}-\text{OH}$ . This process releases an energy of  $271.6\text{ kcal mol}^{-1}$ , which suggests that the reaction trend is thermodynamically very favorable. Therefore, it is not surprising that the DMPO- $\text{GO}_a^{\cdot}-\text{O}^{\cdot}$  peaks in the ESR signal slowly disappeared. Similarly,  $\text{GO}_a-\text{OH}$  also underwent a photoexcitation process to the  $T_1$  state. To initiate the final step ( $\text{GO}_a-\text{OH} \rightarrow \text{GO}_a^{\cdot} + \text{HO}^{\cdot}$ ), however, at least  $79.2\text{ kcal mol}^{-1}$  of

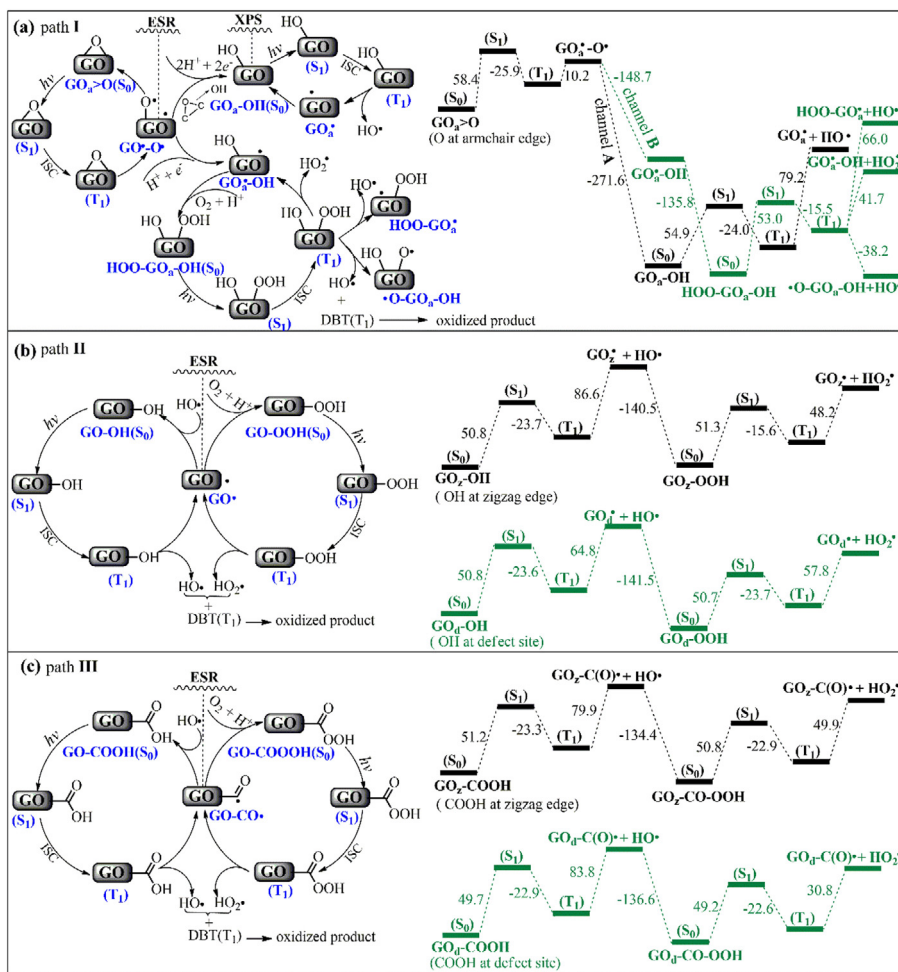


**Fig. 12.** Proposed reaction paths and interaction energies (in  $\text{kcal mol}^{-1}$ ) for (a)  $\text{GO}_a > \text{O}$ , (b)  $\text{GO}-\text{OH}$ , and (c)  $\text{GO}-\text{COOH}$  at the M062X/6–311+G(d,p) level in MeCN. Optimized geometric structures and absolute energies for possible neutral and radical molecules are given in Fig. S9 in SI.

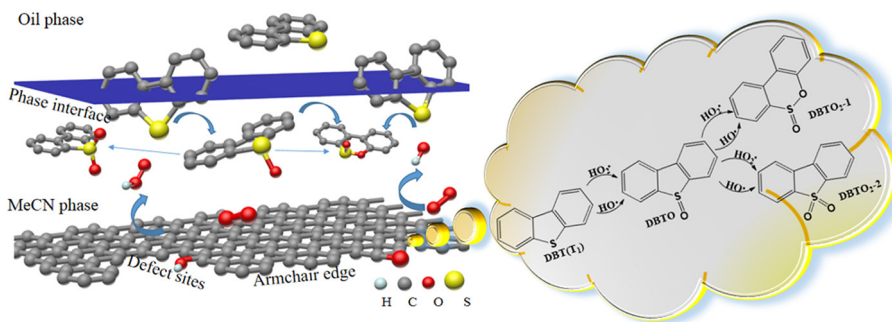
the reaction energy was required, which was higher than that of channel **B** ( $66.0 \text{ kcal mol}^{-1}$ ). This clearly suggests that the dissociation step of  $\text{GO}_a-\text{OH}$  was energetically unfavorable. Specifically,  $\text{GO}_a-\text{OH}$  transformed from  $\text{GO}_a > \text{O}$  and accumulated, which was consistent with the aforementioned epoxy reduction and the increase of  $\text{C}-\text{OH}$  in the spent GO derived from XPS. Channel **B** is:  $\text{GO}_a^{\bullet}-\text{O}^{\bullet} + \text{H}^{\bullet} + e^- \rightarrow \text{GO}^{\bullet}-\text{OH}$ ,  $\text{GO}^{\bullet}-\text{OH} + \text{O}_2 + \text{H}^{\bullet} + e^- \rightarrow \text{HOO}-\text{GO}_a-\text{OH}$ . This channel gives the stable intermediate  $\text{HOO}-\text{GO}_a-\text{OH}$  via two steps with a total interaction energy of  $-284.5 \text{ kcal mol}^{-1}$ . Similarly,  $\text{HOO}-\text{GO}_a-\text{OH}$  also underwent a photoexcitation process to the  $\text{T}_1$  state. As shown in Fig. 12a,  $\text{HOO}-\text{GO}_a-\text{OH}(\text{T}_1)$  might form three kinds of carbon radicals ( $^{\bullet}\text{O}-\text{GO}_a-\text{OH}$ ,  $\text{GO}_a^{\bullet}-\text{OH}$ , and  $\text{HOO}-\text{GO}_a^{\bullet}$ ) through different cleavage modes, and the corresponding reaction energies were  $-38.2 \text{ kcal mol}^{-1}$ ,  $41.7 \text{ kcal mol}^{-1}$ , and  $66.0 \text{ kcal mol}^{-1}$ , respectively. It was clear that the direction of the reaction proceeded along  $\text{HOO}-\text{GO}_a-\text{OH} \rightarrow ^{\bullet}\text{O}-\text{GO}_a-\text{OH} + \text{HO}^{\bullet}$ , because this reaction did not require additional energy. To further confirm whether the reaction had a transition state, a potential energy profile was scanned along the  $\text{O}-\text{O}$  distance. As shown in Fig. S8, only one possible transition state existed in the reaction coordinates, and the energy barrier was  $3.6 \text{ kcal mol}^{-1}$ . Overall, the channel for generating  $^{\bullet}\text{O}-\text{GO}_a-\text{OH}$  and  $\text{HO}^{\bullet}$  from  $\text{GO}_a > \text{O}$  was the most energetically favorable in path **I**.

In path **II** (Fig. 12b),  $\text{GO}-\text{OH}(\text{T}_1) \rightarrow \text{GO}^{\bullet} + \text{HO}^{\bullet}$  was the rate-determining step according to the required reaction energies. Clearly,  $\text{GO}_d-\text{OH}$  was an energetically favorable channel that overcame the reaction energy of  $64.8 \text{ kcal mol}^{-1}$  with respect to

$86.6 \text{ kcal mol}^{-1}$  of  $\text{GO}_z-\text{OH}$ . In path **III** (Fig. 12c), however, the reaction energies at the rate-determining steps of  $\text{GO}_z-\text{COOH}$  and  $\text{GO}_d-\text{COOH}$  were  $79.9 \text{ kcal mol}^{-1}$  and  $83.8 \text{ kcal mol}^{-1}$ , respectively, both of which were higher than that of  $\text{GO}_d-\text{OH}$  in path **II**. This indicates that path **III** was energetically unfavorable. Thus  $\text{COOH}$  showed negligible change after reaction, which was confirmed by ATR FT-IR and XPS analysis. Overall,  $\text{GO}_d-\text{OH}$  with absorbed  $\text{O}_2$  and  $\text{H}^{\bullet}$  was the main source of  $\text{HO}^{\bullet}$  and  $\text{HO}_2^{\bullet}$ , which further oxidized DBT to products [35].

On the whole, the proposed paths **I** and **II** for forming ROS were predicted using DFT calculations. These were in good agreement with the above-mentioned experimental observations and also supported the previous findings that the oxygen from functional groups and absorbed  $\text{O}_2$  on nanoporous carbons are the only driving force for the oxidation of DBT [85].

After reaction, the MeCN phase was separated and diluted 20 times with ethanol to study the photocatalytic oxidizing products using GC-MS. As shown in Fig. S10, there are several peaks in the total ion chromatogram, indicating that complicated products were obtained by the oxidation of DBT. According to the mass spectra, the molecular ion peaks of the two main compounds at 7.95 min and 8.46 min were attributed to dibenzo[c,e][1,2]oxathiine 6-oxide (DBTO<sub>2</sub>-1) and dibenzo[b,d]thiophene 5,5-dioxide (DBTO<sub>2</sub>-2), respectively, although other peaks could not be clearly identified. DBTO<sub>2</sub>-2 is commonly referred to as dibenzothiophene sulfone, which has been a frequently observed product in previous thermocatalytic or photocatalytic ODS studies [12,35,58].



**Scheme 1.** Schematic depiction of the desulfurization process using GO in the presence of O<sub>2</sub> under UV radiation.

Based on the above-mentioned results of ESR, DFT, and GC–MS analyses, a proposed mechanism is depicted in **Scheme 1**. The model oil, GO, MeCN, and MeA formed a heterogeneous catalytical system. At the beginning of reaction, DBT was initially extracted into the MeCN phase and then oxidized by HO<sub>2</sub><sup>•</sup> and HO<sup>•</sup> produced from the defect sites and the zigzag edge of GO. The stepwise oxidation mechanism for the reactions process has been widely accepted by previous studies [35,86]. DBT is first oxidized to the corresponding sulfoxide (DBTO) by HO<sub>2</sub><sup>•</sup> and HO<sup>•</sup> and then to DBTO<sub>2</sub>-1 and DBTO<sub>2</sub>-2, which remain in the MeCN phase because of their high polarity. Ultra-low sulfur model oil was obtained when DBT was transferred from the oil phase to the MeCN phase and continuously oxidized to DBTO<sub>2</sub>.

#### 4. Conclusions

In summary, a simple extraction and photocatalytic oxidative desulfurization (EPODS) system for model oil was successfully developed, on the basis of GO, air, MeA, and MeCN. The main reaction conditions were assessed, including the amount of GO, the volume ratio of MeCN to model oil ( $r_{M/o}$ ), the amount of MeA, the initial S-concentration, air/N<sub>2</sub> bubbling, different sulfur compounds, and fuel composition. The results demonstrated that the EPODS had an optimal photocatalytic performance with a GO dosage of 0.6 mg,  $r_{M/o}$  of 1:2, MeA of 4.5 mL, and air at a rate of 20 mL min<sup>-1</sup>. Sulfur removal from BT, DBT, and 4,6-DMDBT were 100%, 99.9%, and 99.4%, respectively, in 140 min. The corresponding reactivity differences were attributed to the influences of both the electronic structure of the lowest-lying triplet state of each species and steric hindrance. The oxygen-containing functional groups in GO along with the absorbed O<sub>2</sub>, the ambient H<sup>+</sup>, and additional electrons formed carbon radicals (GO<sup>•</sup> and GO<sup>•-</sup>) and ROS (HO<sub>2</sub><sup>•</sup> and HO<sup>•</sup>), which mainly originated from the zigzag edge and the defect sites. HO<sub>2</sub><sup>•</sup> and HO<sup>•</sup> were responsible for the oxidation of the DBT initially extracted into the MeCN phase, and then the mixed oxidation products, including sulfone, remained in the MeCN phase because of their high polarity, thus achieving deep desulfurization. Therefore, this study inspires the exploration of similar EPODS systems by constructing an innovative carbon photocatalyst for wider applications in clean fuel production technology.

#### Acknowledgements

This work was supported by the National Natural Science Foundation of China (Grant No. 21376099, 21403038, 21546002), the Natural Science Foundation of Guangdong Province (Grant No. 2015A030313892), the Training Program for Outstanding Young Teachers in Colleges and Universities in Guangdong Province (Grant No. YQ2015116).

#### Appendix A. Supplementary data

Supplementary data associated with this article can be found, in the online version, at <http://dx.doi.org/10.1016/j.apcatb.2017.02.077>.

#### References

- [1] A. Stanislaus, A. Marafi, M.S. Rana, *Catal. Today* 153 (2010) 1–68.
- [2] R. Ullah, P. Bai, P. Wu, Z. Zhang, Z. Zhong, U.J. Etim, F. Subhan, Z. Yan, *Energy Fuel* 30 (2016) 2874–2881.
- [3] I. Shimoyama, Y. Baba, *Carbon* 98 (2016) 115–125.
- [4] United States Environmental Protection Agency (USEPA), EPA-420-F-14-009, 2014.
- [5] G.I. Danmaliki, T.A. Saleh, *J. Clean. Prod.* 117 (2016) 50–55.
- [6] Z. Varga, Z. Eller, J. Hancsok, *J. Clean. Prod.* 111 (2016) 108–116.
- [7] F.T. Li, B. Wu, R.H. Liu, X.J. Wang, L.J. Chen, D.S. Zhao, *Chem. Eng. J.* 274 (2015) 192–199.
- [8] X.D. Tang, Y.F. Zhang, J.J. Li, Y.Q. Zhu, D.Y. Qing, Y.X. Deng, *Ind. Eng. Chem. Res.* 54 (2015) 4625–4632.
- [9] S. Escobar, A. Rodriguez, E. Gomez, A. Alcon, V.E. Santos, F. Garcia-Ochoa, *Bioproc. Biosyst. Eng.* 39 (2016) 545–554.
- [10] L. Li, J. Zhang, C. Shen, Y. Wang, G. Luo, *Fuel* 167 (2016) 9–16.
- [11] A.D. Bokare, W. Choi, J. Hazard. Mater. 304 (2016) 313–319.
- [12] W. Zhu, B. Dai, P. Wu, Y. Chao, J. Xiong, S. Xun, H. Li, H. Li, *ACS Sustain. Chem. Eng.* 3 (2015) 186–194.
- [13] H.Y. Sun, L.P. Sun, F. Li, L. Zhang, *Fuel Process. Technol.* 134 (2015) 284–289.
- [14] Y. Shi, X. Zhang, G. Liu, *Fuel* 158 (2015) 565–571.
- [15] J. Xiao, S. Sitamraju, Y. Chen, S. Watanabe, M. Fujii, M. Janik, C. Song, *AIChE J.* 61 (2015) 631–639.
- [16] B. Dai, P. Wu, W. Zhu, Y. Chao, J. Sun, J. Xiong, W. Jiang, H. Li, *RSC Adv.* 6 (2016) 140–147.
- [17] H.Y. Lu, P.C. Li, C.L. Deng, W.Z. Ren, S.N. Wang, P. Liu, H. Zhang, *Chem. Commun.* 51 (2015) 10703–10706.
- [18] S. Li, N. Mominou, Z. Wang, L. Liu, L. Wang, *Energy Fuel* 30 (2016) 962–967.
- [19] H. Lu, J. Gao, Z. Jiang, Y. Yang, B. Song, C. Li, *Chem. Commun. (Camb.)* (2007) 150–152.
- [20] P. Wu, W. Zhu, A. Wei, B. Dai, Y. Chao, C. Li, H. Li, S. Dai, *Chem. Eur. J.* 21 (2015) 15421–15427.
- [21] J. Wang, D. Zhao, K. Li, *Energy Fuel* 24 (2010) 2527–2529.
- [22] C. Ma, D. Chen, F. Liu, X. Sun, F. Xiao, B. Dai, *RSC Adv.* 5 (2015) 96945–96952.
- [23] Y.Y. Ma, H.Q. Tan, Y.H. Wang, X.L. Hao, X.J. Feng, H.Y. Zang, Y.G. Li, *Crystengcomm* 17 (2015) 7938–7947.
- [24] M.Y. Masoomi, M. Bagheri, A. Morsali, *Inorg. Chem.* 54 (2015) 11269–11275.
- [25] J.T. Sampantan, H. Xiao, J. Dou, T.Y. Nah, X. Rong, W.P. Kwan, *Appl. Catal. B Environ.* 63 (2006) 85–93.
- [26] A.T. Nawaf, S.A. Ghani, A.T. Jarullah, I.M. Mujtaba, *Fuel Process. Technol.* 138 (2015) 337–343.
- [27] X. Ma, A. Zhou, C. Song, *Catal. Today* 123 (2007) 276–284.
- [28] K.M. Dooley, D. Liu, A.M. Madrid, F.C. Knopf, *v Appl. Catal. A Gen.* 468 (2013) 143–149.
- [29] H. Lu, W. Ren, W. Liao, W. Chen, Y. Li, Z. Suo, *Appl. Catal. B Environ.* 138 (2013) 79–83.
- [30] W. Zhang, J. Xiao, X. Wang, G. Miao, F. Ye, Z. Li, *Energy Fuel* 28 (2014) 5339–5344.
- [31] R. Sundararaman, C. Song, *Ind. Eng. Chem. Res.* 53 (2014) 1890–1899.
- [32] F. Lin, D. Wang, Z. Jiang, Y. Ma, J. Li, R. Li, C. Li, *Energy Environ. Sci.* 5 (2012) 6400–6406.
- [33] F. Lin, Y. Zhang, L. Wang, Y. Zhang, D. Wang, M. Yang, J. Yang, B. Zhang, Z. Jiang, C. Li, *Appl. Catal. B Environ.* 127 (2012) 363–370.
- [34] H.F. Mohd Zaid, F.K. Chong, M.I. Abdul Mutalib, *Fuel* 156 (2015) 54–62.
- [35] W.S. Zhu, C. Wang, H.P. Li, P.W. Wu, S.H. Xun, W. Jiang, Z.G. Chen, Z. Zhao, H.M. Li, *Green Chem.* 17 (2015) 2464–2472.
- [36] Y. Zhai, Z. Zhu, S. Dong, *Chemcatchem* 7 (2015) 2806–2815.

[37] Q. Liu, Y. Gong, T. Wang, W.-L. Chan, J. Wu, *Carbon* 96 (2016) 203–211.

[38] L. Wang, R.T. Yang, C.-L. Sun, *AIChE J.* 59 (2013) 29–32.

[39] H.S. Song, C.H. Ko, W. Ahn, B.J. Kim, E. Croiset, Z. Chen, S.C. Nam, *Ind. Eng. Chem. Res.* 51 (2012) 10259–10264.

[40] F. Duan, C. Chen, G. Wang, Y. Yang, X. Liu, Y. Qin, *RSC Adv.* 4 (2014) 1469–1475.

[41] G.A.B. Gonçalves, S.M.G. Pires, M.M.Q. Simões, M.G.P.M.S. Neves, P.A.A.P. Marques, *Chem. Commun.* 50 (2014) 7673–7676.

[42] C. Su, K.P. Loh, *Acc. Chem. Res.* 46 (2013) 2275–2285.

[43] D.R. Dreyer, H.P. Jia, C.W. Bielawski, *Angew. Chem.* 49 (2010) 6813–6816.

[44] Y. Pan, S. Wang, C.W. Kee, E. Dubuisson, Y. Yang, K.P. Loh, C.-H. Tan, *Green Chem.* 13 (2011) 3341–3344.

[45] Y. Jiao, Y. Zheng, M. Jaroniec, S.Z. Qiao, *J. Am. Chem. Soc.* 136 (2014) 4394–4403.

[46] T. Yanai, D.P. Tew, N.C. Handy, *Chem. Phys. Lett.* 393 (2004) 51–57.

[47] Y. Zhao, D.G. Truhlar, *Theor. Chem. Acc.* 120 (2008) 215–241.

[48] M.J. Frisch, et al., Gaussian 09, Revision D.01, Gaussian, Inc., Wallingford CT, 2013.

[49] J. Tomasi, B. Mennucci, R. Cammi, *Chem. Rev.* 105 (2005) 2999–3093.

[50] E. Runge, E.K.U. Gross, *Phys. Rev. Lett.* 52 (1984) 997–1000.

[51] D. Mandal, K. Sen, A.K. Das, *J. Phys. Chem. A* 116 (2012) 8382–8396.

[52] B.R. Moser, R.L. Evangelista, T.A. Isbell, *Energy Fuel* 30 (2016) 473–479.

[53] A. Samokhvalov, *Catal. Rev.* 54 (2012) 281–343.

[54] H. Mirhoseini, M. Taghdiri, *Fuel* 167 (2016) 60–67.

[55] X.J. Wang, F.T. Li, J.X. Liu, C.G. Kou, Y. Zhao, Y.J. Hao, D. Zhao, *Energy Fuel* 26 (2012) 6777–6782.

[56] J. Xiao, S. Sitamraju, S. Watanabe, M. Fujii, Y. Chen, M. Janik, C. Song, *Langmuir* 30 (2014) 1080–1088.

[57] X.M. Gao, F. Fu, L.P. Zhang, W.-H. Li, *Physica B* 419 (2013) 80–85.

[58] W. Zhang, H. Zhang, J. Xiao, Z.X. Zhao, M.X. Yu, Z. Li, *Green Chem.* 16 (2014) 211–220.

[59] T. Hirai, Y. Shiraishi, K. Ogawa, I. Komasawa, *Ind. Eng. Chem. Res.* 36 (1997) 530–533.

[60] Y. Shiraishi, Y. Taki, T. Hirai, I. Komasawa, *Ind. Eng. Chem. Res.* 38 (1999) 3310–3318.

[61] T.D. Nguyen-Phan, S. Luo, Z. Liu, A.D. Gamalski, J. Tao, W. Xu, E.A. Stach, D.E. Polyansky, S.D. Senanayake, E. Fujita, J.A. Rodriguez, *Chem. Mater.* 27 (2015) 6282–6296.

[62] J. Bu, G. Loh, C.G. Gwie, S. Dewiyanti, M. Tasrif, A. Borgna, *Chem. Eng. J.* 166 (2011) 207–217.

[63] S. Otsuki, T. Nonaka, N. Takashima, W. Qian, A. Ishihara, T. Imai, T. Kabe, *Energy Fuel* 14 (2000) 1232–1239.

[64] Y. Jia, G. Li, G. Ning, *Fuel Process. Technol.* 92 (2011) 106–111.

[65] W. Zhu, Y. Xu, H. Li, B. Dai, H. Xu, C. Wang, Y. Chao, H. Liu, *Korean J. Chem. Eng.* 31 (2014) 211–217.

[66] D. Zheng, W.S. Zhu, S.H. Xun, M.M. Zhou, M. Zhang, W. Jiang, Y.J. Qin, H.M. Li, *Fuel* 159 (2015) 446–453.

[67] S. Xun, W. Zhu, D. Zheng, H. Li, W. Jiang, M. Zhang, Y. Qin, Z. Zhao, H. Li, *RSC Adv.* 5 (2015) 43528–43536.

[68] S. Xun, W. Zhu, Y. Chang, H. Li, M. Zhang, W. Jiang, D. Zheng, Y. Qin, H. Li, *Chem. Eng. J.* 288 (2016) 608–617.

[69] C. Wang, W. Zhu, Z. Chen, S. Yin, P. Wu, S. Xun, W. Jiang, M. Zhang, H. Li, *RSC Adv.* 5 (2015) 99927–99934.

[70] H. Li, W. Zhu, Y. Wang, J. Zhang, J. Lu, Y. Yan, *Green Chem.* 11 (2009) 810.

[71] C. Ma, B. Dai, P. Liu, N. Zhou, A. Shi, L. Ban, H. Chen, *J. Ind. Eng. Chem.* 20 (2014) 2769–2774.

[72] Y. Shiraishi, K. Tachibana, T. Hirai, I. Komasawa, *Ind. Eng. Chem. Res.* 41 (2002) 4362–4375.

[73] O. Acevedo, W.L. Jorgensen, *Acc. Chem. Res.* 43 (2010) 142–151.

[74] V. Etacheri, C. Di Valentin, J. Schneider, D. Bahnemann, S.C. Pillai, J. *Photochem. Photobiol. C* 25 (2015) 1–29.

[75] K.A. Kurnia, M.V. Quental, L. Santos, M.G. Freire, J.A.P. Coutinho, *Phys. Chem. Chem. Phys.* 17 (2015) 4569–4577.

[76] K. Fukui, *Science* 218 (1982) 747–757.

[77] M. Bobrowski, A. Liwo, K. Hirao, *J. Phys. Chem. B* 111 (2007) 3543–3549.

[78] Y. Liu, H. Guo, Y. Zhang, W. Tang, X. Cheng, H. Liu, *Chem. Phys. Lett.* 653 (2016) 101–107.

[79] J.J. Salazar-Rabago, M. Sanchez-Polo, J. Rivera-Utrilla, R. Leyva-Ramos, R. Ocampo-Perez, F. Carrasco-Marín, *Chem. Eng. J.* 306 (2016) 289–297.

[80] L. Yang, R. Zhang, B. Liu, J. Wang, S. Wang, M.-Y. Han, Z. Zhang, *Angew. Chem. Int. Ed.* 53 (2014) 10109–10113.

[81] D.W. Boukhvalov, V.Y. Osipov, A.I. Shames, K. Takai, T. Hayashi, T. Enoki, *Carbon* 107 (2016) 800–810.

[82] W. Zou, L. Zhang, L. Liu, X. Wang, J. Sun, S. Wu, Y. Deng, C. Tang, F. Gao, L. Dong, *Appl. Catal. B Environ.* 181 (2016) 495–503.

[83] F. Chen, Q. Yang, X. Li, G. Zeng, D. Wang, C. Niu, J. Zhao, H. An, T. Xie, Y. Deng, *Appl. Catal. B Environ.* 200 (2017) 330–342.

[84] S. Navalon, A. Dhakshinamoorthy, M. Alvaro, H. Garcia, *Chem. Rev.* 114 (2014) 6179–6212.

[85] M. Seredych, T.J. Bandosz, *Carbon* 49 (2011) 1216–1224.

[86] J.M. Yin, J.P. Wang, Z. Li, D. Li, G. Yang, Y.N. Cui, A.L. Wang, C.P. Li, *Green Chem.* 17 (2015) 4552–4559.